Pramāṇa, Vol. 15, No. 2, August 1980, pp. 207-223. © Printed in India.

Magnetic moment distributions and form factors in ferromagnetic nickel-ruthenium alloys

R CHAKRAVARTHY, L MADHAV RAO and
N S SATYA MURTHY
Nuclear Physics Division, Bhabha Atomic Research Centre,
Trombay, Bombay 400 085, India

MS received 9 May 1980; revised 11 July 1980

Abstract. Using polarised neutrons, the full three-dimensional magnetic structure amplitudes in the Ni_{1-c} Ru_c single crystals for $c = 0{\cdot}027$, $0{\cdot}033$ and $0{\cdot}046$ were measured. Moment density maps in various portions of the Wigner-Seitz cell were obtained. It is seen from these maps that unlike Ni-based alloys with 3*d* impurities, the introduction of Ru to the Ni matrix produces extensive perturbations in the diffuse moment density, giving rise to a net *positive* diffuse moment which tends to increase with Ru concentration. The asphericity of the host moment at first increases and then decreases with increasing Ru content. Another significant outcome of the present study is the evidence for the reversal of the sign of the Ru moment, from negative to positive, obtained by comparing the shape of the spherical site form factors of the three-alloy concentrations with the Ni spherical form factor itself. The sign reversal of the impurity moment is confirmed by the form factor analyses. Strong local environmental effects seem to play a major role in this alloy system.

Keywords. Magnetic moment density; polarised neutron diffraction; magnetic form factors; ferromagnetic dilute alloys; nickel-ruthenium alloys; form factors.

1. Introduction

The polarised neutron diffraction technique is a precise and powerful tool to map out the detailed moment density distributions in magnetic crystals. The early measurements done on the 3*d* elements—Fe, Co and Ni showed these spin density distributions to be characterized by large positive densities localised at the atomic sites riding over a uniform negative diffuse density (Shull and Yamada 1962; Moon 1964; Mook 1966). Subsequently attention was focussed on the detailed concentration dependence of the moment distributions, the asphericity of the local moment and diffuse moment density in a variety of dilute ferromagnetic 3*d*—3d alloys (Dobrzynski *et al* 1970; Ito and Akimitsu 1974; Livet and Radhakrishna 1976). The general picture that emerged from these polarised neutron studies was that with the increase of impurity concentration, there was a tendency for the asphericity of the local moment to decrease, while the interstitial diffuse moment density continued to be uniformly negative with very little dependence on the impurity concentration. Similar studies in 3*d*-based alloys with dilute 4*d* impurities have not been reported so far.

We describe here a polarised neutron study on a series of single crystals of nickel-ruthenium alloys with Ru concentration varying from 2·7 at. % to 4·6 at. %. (A portion of this work was reported earlier, vide Madhav Rao *et al* 1978, hereafter referred to as I). This particular 3*d*-4*d* dilute system was chosen for our study be-

cause transport property measurements in the Ni Ru alloys (Durand and Gautier 1970; Cadeville and Roussel 1971) gave indirect evidence of the formation of an impurity virtual bound state very near the Fermi level E_f. In this picture, one should expect to find fairly extensive magnetic perturbations in the lattice.

2. Experimental

Single crystals of three-alloy concentration were studied. The exact composition of these alloys was established by x-ray fluorescence and were found to be $Ni_{0.973}$ $Ru_{0.027}$, $Ni_{0.967}$ $Ru_{0.033}$ and $Ni_{0.954}$ $Ru_{0.046}$. These were cross-checked again by electron microprobe analysis. For each of these alloys, several small specimens were cut by spark erosion from a large single crystal. The specimens were in the form of parallelopipeds of height approximately 8 mm, width 2 to 3 mm and thickness varying from 0·2 to 0·6 mm. In each case, the zone axis was adjusted to be along the longest dimension. Special angular cuts were made such that different equivalents of the same reflection had different neutron path lengths in order to enable a proper evaluation of extinction effects in the crystal. From the positions of the high angle Bragg reflections, the lattice constants in these alloys were found to be nearly the same as in nickel ($a_0 \simeq 3{\cdot}524$ Å) to within 1 to 2%.

The polarisation ratios (R) were measured on these thin crystal specimens on the polarised neutron spectrometer at the CIRUS reactor, BARC. All measurements were done at room temperature in a magnetizing field of 7 kOe and neutron wave length of 0·92 Å. For each of the alloy concentration, polarisation ratios for 64 reflections including 16 independent ones were measured in the (110), (001) and (112) zones upto $\sin\theta/\lambda = 0{\cdot}9$ Å^{-1}. The observed polarisation ratios (vide equation (1) of I) were corrected for incomplete incident neutron polarisation (~6%), flipping efficiency of the RF flipper (~1%) and for specimen depolarisation. We checked for the presence of multiple Bragg effects by measuring the polarisation ratios of the more susceptible reflections in different zones and such effects were found to be negligible.

The procedure for extracting the magnetic structure amplitudes from the observed polarisation ratios taking into account the instrumental parameters and correcting for secondary extinction and depolarisation of the incident beam as outlined in I, was carried out. In each of the alloy specimens in increasing order of the Ru concentration the depolarisation coefficient μ was experimentally determined to be 0·008 cm^{-1}, 0·012 cm^{-1} and 0·011 cm^{-1}. In the least squares analysis of the data all the three alloy crystals were found to be affected by type I (mosaic-dominated) secondary extinction. The values of the extinction parameter g obtained in these alloys (in increasing order of Ru content) were $0{\cdot}137 \times 10^4$, $0{\cdot}025 \times 10^4$ and $0{\cdot}089 \times 10^4$. Tables 1 to 3 summarise the results of the analysis. The R_{cal} column in these tables include extinction effects. Though 64 reflections were used in the analysis for each alloy composition, only those reflections whose equivalents have widely different neutron pathlengths have been shown. However, the M/N values and the M values shown in the last two columns are averaged values over all the equivalents of the Bragg reflection. Primary extinction effects were not specifically evaluated, but from the good fits we obtained, we believe these effects, if present at all, to be insignificant compared to secondary extinction.

Table 1. Summary of the measured polarisation ratios in various specimen of $Ni_{0.973}$ $Ru_{0.027}$ alloy. Specimen thicknesses are 1:0·6 mm, 2:0·3 mm, 3:0·25 mm, M, the magnetic structure amplitude is in μ_s per atom. N the nuclear structure amplitude is $1{\cdot}022 \times 10^{-12}$ cm. g the extinction parameter in $0{\cdot}137 \times 10^4$.

(*hkl*)	Zone and specimen	Neutron path-length (cm)	R_{obs}	R_{cal}	M/N	M
(11$\bar{1}$)	[110], 1	0·1682	1·217	1·211		
					0·0916 (7)	0·347 (3)
(11$\bar{1}$)	[110], 2	0·1038	1·221	1·225		
(200)	[110], 1	0·0619	1·216	1·213	0·0794 (7)	0·301 (3)
(220)	[110], 1	0·1273	1·137	1·127		
					0·0525 (5)	0·199 (2)
(220)	[110], 2	0·0691	1·141	1·141		
(311)	[110], 1	0·0564	1·111	1·113		
					0·0397 (5)	0·151 (2)
($\bar{3}$11)	[110], 1	0·1321	1·106	1·096		
(222)	[110], 1	0·0654	1·116	1·117	0·0424 (6)	0·160 (2)
(400)	[110], 1	0·0766	1·057	1·053	0·0201 (9)	0·076 (3)
(33$\bar{1}$)	[110], 1	0·1037	1·054	1·056	0·0221 (7)	0·084 (3)
(420)	[100], 3	0·0251	1·060	1·060	0·0157 (9)	0·060 (3)
(422)	[110], 1	0·0662	1·042	1·042	0·0154 (7)	0·058 (3)
(511)	[110], 1	0·1469	1·011	1·014		
					0·0059 (6)	0·022 (2)
(511)	[110], 2	0·0741	1·017	1·016		
($\bar{5}$33)	[110], 1	0·0855	1·037	1·036	0·0138 (6)	0·052 (2)
(440)	[110], 1	0·0984	1·014	1·014	0·0057 (10)	0·022 (4)
(531)	[112], 1	0·1000	1·010	1·010	0·0041 (10)	0·016 (4)
(600)	[110], 1	0·1331	0·9878	0·9878	(—) 0·0052 (12)	(—) 0·020 (5)
(442)	[110], 1	0·0664	1·017	1·022	0·0079 (8)	0·030 (3)
(620)	[100], 3	0·1232	0·999	0·999	(—) 0·0002 (13)	(—) 0·001 (5)

Table 2. Summary of the polarisation ratios in various specimens of $Ni_{0.967}$ $Ru_{0.033}$ alloy. Specimen thicknesses are: 1:0·3 mm, 2:0·2 mm, N, the nuclear structure amplitude is $1{\cdot}020 \times 10^{-12}$ cm, g the extinction parameter is $0{\cdot}024 \times 10^4$.

(*hkl*)	Zone and specimen	Neutron path length (cm)	R_{obs}	R_{cal}	M/N	M
(111)	[110], 1	0·0275	1·308	1·315	0·0804 (9)	0·304 (3)
(11$\bar{1}$)	[110], 1	0·0976	1·271	1·266		
(200)	[001], 2	0·0559	1·261	1·266	0·0733 (5)	0·278 (2)
(220)	[110], 1	0·0653	1·154	1·155	0·0448 (7)	0·170 (3)
(311)	[110], 1	0·0279	1·126	1·129		
					0·0344 (6)	0·130 (2)
($\bar{3}$11)	[110], 1	0·1082	1·114	1·113		
($\bar{2}$22)	[110], 1	0·0533	1·123	1·124	0·0345 (6)	0·131 (2)
(400)	[110], 1	0·0411	1·058	1·058	0·0162 (6)	0·061 (2)
($\bar{3}$31)	[110], 1	0·0623	1·067	1·061	0·0177 (5)	0·067 (2)
(420)	[001], 2	0·0616	1·047	1·047	0·0136 (6)	0·051 (2)
(422)	[110], 1	0·0322	1·039	1·044	0·0120 (5)	0·046 (2)
(511)	[110], 1	0·0384	1·018	1·016	0·0044 (4)	0·017 (1)
(333)	[110], 1	0·0406	1·042	1·041	0·0113 (5)	0·043 (2)
(440)	[110], 1	0·0608	1·022	1·022	0·0063 (7)	0·024 (3)
(531)	[112], 1	0·1000	1·009	1·009	0·0028 (9)	0·011 (3)
(600)	[110], 1	0·1117	0·9884	0·9884	(—) 0·0037 (8)	(—) 0·014 (3)
(442)	[110], 1	0·0337	1·020	1·016	0·0044 (6)	0·017 (2)
(620)	[001], 2	0·0740	0·9971	0·9971	(—) 0.0009 (9)	(—) 0·003 (3)

Table 3. Summary of the measured polarisation ratios in two specimens of the $Ni_{0.954}Ru_{0.046}$ alloy. Specimen thicknesses are: 1:0·2 mm, 2:0·35 mm, N, the nuclear scattering amplitude is $1{\cdot}016 \times 10^{-12}$ cm, g the extinction parameter is $0{\cdot}089 \times 10^{4}$.

(*hkl*)	Zone and specimen	Neutron path length (cm)	R_{obs}	R_{cal}	M/N	M
(111)	[1̄10], 1	0·0320	1·272	1·276	0·0662 (4)	0·250 (1)
(200)	[110], 1	0·0278	1·250	1·243	0·0593 (5)	0·224 (2)
(220)	[001], 2	0·1172	1·096	1·097	0.0374 (5)	0·141 (2)
(2̄20)	[001], 2	0·0582	1·112	1·110		
(3̄11)	[110], 2	0·0314	1·095	1·094	0·0244 (2)	0·092 (1)
(222)	[110], 1	0·0390	1·092	1·091	0·0236 (2)	0·089 (1)
(400)	[110], 1	0·0264	1·052	1·054	0·0142 (5)	0·053 (2)
(331)	[110], 1	0·1042	1·055	1·050	0·0133 (4)	0·050 (1)
(420)	[001], 2	0·0702	1·032	1·033	0·0113 (6)	0·043 (2)
(422)	[110], 1	0·0354	1·036	1·034	0·0091 (4)	0·034 (1)
(511)	[110], 1	0·0294	1·016	1·015	0·0040 (4)	0·015 (1)
(3̄33)	[110], 1	0·0374	1·033	1·032	0·0086 (4)	0·033 (1)
(440)	[001], 2	0·1300	1·014	1·015	0·0057 (3)	0·021 (1)
(4̄40)	[001], 2	0·0701	1·020	1·016		
(531)	[112], 2	0·1100	1·011	1·011	0·0041 (11)	0·015 (4)
(600)	[110], 1	0·0280	0·9951	0·9951	(—) 0·0018 (7)	(—) 0·007 (3)
(44̄2)	[110], 1	0·0430	1·015	1·017	0·0044 (4)	0·017 (1)
(620)	[001], 2	0·1175	0·9985	0·9983	(—) 0·0007 (8)	(—) 0·003 (3)
(6̄20)	[001], 2	0·0761	0·9979	0·9981		

3. Analysis

3.1 *Moment density maps*

The magnetic structure amplitudes M shown in tables 1-3, are the coefficients of the Fourier decomposition of the periodic magnetization density in real space. The most direct method of analysis is to perform the Fourier sum of the measured magnetic structure amplitudes to get the point density distribution $\rho(\mathbf{r})$ at all r's in the unit cell. The first term in this sum is the magnetic structure amplitude associated with the (000) reflection, which is obtained from the bulk moment measurements on the alloy sample. The bulk moment per site atom (measured in a vibrating sample magnetometer) in the three alloys were found to be 0·505 μ_B, 0·473 μ_B, and 0·404 μ_B. The finite number of magnetic structure amplitudes produces unphysical oscillations in the point density, especially in the regions far removed from the atomic site. It is hence customary to define an average moment density

$$\overline{\rho(\mathbf{r})} = \frac{1}{V_0} \sum_j M_j' \exp(-i\mathbf{k}_j \cdot \mathbf{r}) \tag{1}$$

in which

$$M'_{hkl} = \frac{M_{hkl}}{hkl\,(2\pi\delta)^3} \sin(2\pi h\delta) \sin(2\pi k\delta) \sin(2\pi l\delta). \tag{2}$$

That is, the point density $\rho(\mathbf{r})$ is averaged over a miniature cubic cell of linear dimension $2a\,\delta$. Following Moon (1971), point density contours were obtained near and around the atomic sites where $\rho(\mathbf{r})$ varies sharply with $\mathbf{r}$, while in the interstitial regions, miniature cell averaging of $\rho(\mathbf{r})$ was resorted to with $\delta = 0{\cdot}08$. Moment density maps were obtained in different planes in the crystal. Figures 1 to 3 show these maps in the $(1\bar{1}0)$ plane for the three-alloy concentrations. It will be interesting to compare the salient features of these maps with those obtained by Mook (1966) in pure Ni. The first feature is the asymmetry of the magnetic contours around the atomic sites. In the alloy with the lowest Ru concentration, these contours are stretched more in the $\langle 110\rangle$ direction than in pure Ni, showing a somewhat larger T_{2g} asymmetry in the spin density distribution. With the increase of Ru concentration one perceives from these maps a 'softening' of this asymmetry. However, the most significant feature of these maps is the fairly strong perturbation introduced by the Ru impurity on the diffuse moment density i.e. in portions of the unit cell far removed from the atomic sites. Whereas Mook observed a uniform negative diffuse

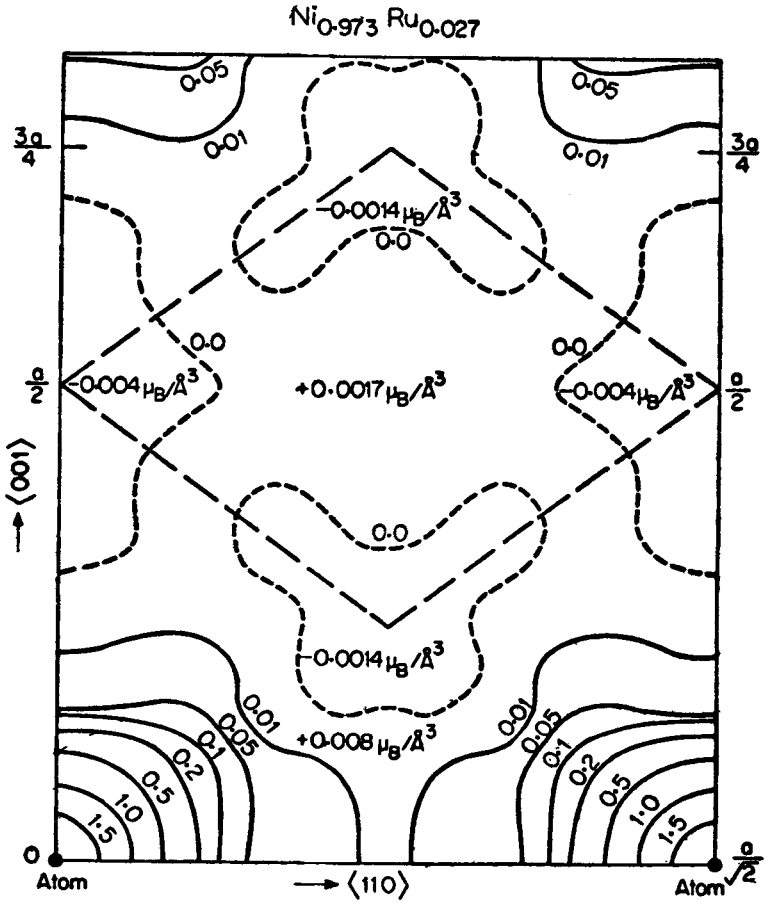

Figure 1. Magnetic moment density map in the $(1\bar{1}0)$ plane in $Ni_{0\cdot973}Ru_{0\cdot027}$. One of the WS cell faces shared by the atoms $\frac{1}{2}\ 0\ \frac{1}{2}$ and $0\ \frac{1}{2}\ \frac{1}{2}$ is shown by the portion enclosed by the broken lines. The error on the diffuse densities is $\pm\ 0{\cdot}0004\ \mu_B/\text{Å}^3$.

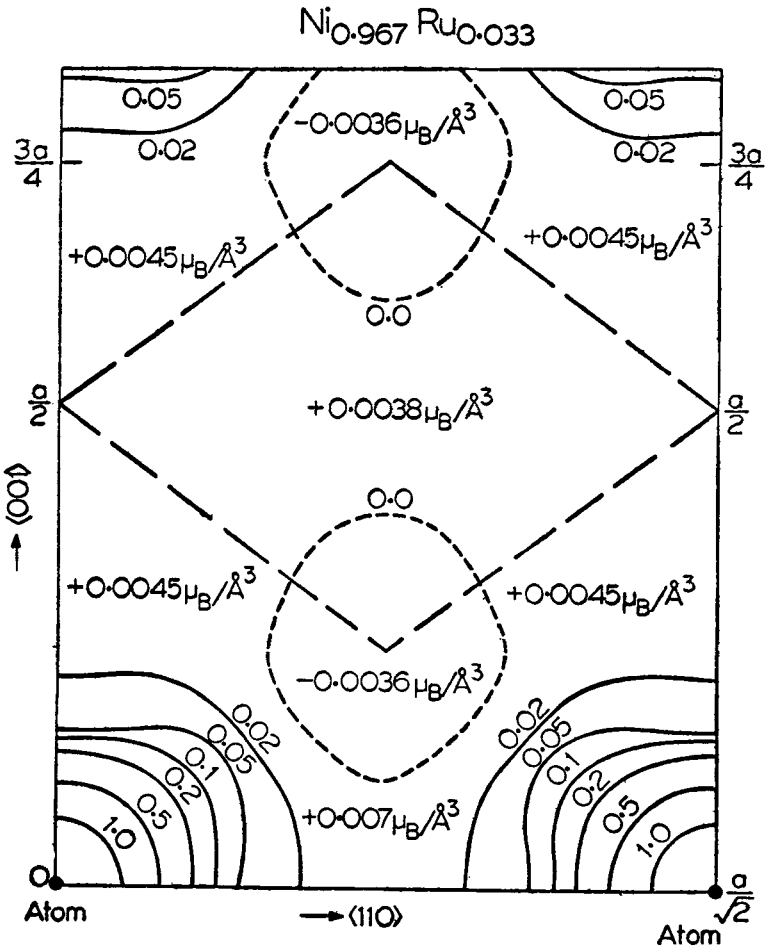

Figure 2. Magnetic moment density map in the (1$\bar{1}$0) plane in $Ni_{0\cdot967}$ $Ru_{0\cdot033}$. The error on the diffuse density is $\pm$ 0·0004 $\mu_B/Å^3$.

moment density of $-0\cdot0085$ $\mu_B/Å^3$ in Ni in these regions, we observe here islands of positive and negative diffuse moments in these maps, which is especially striking in the alloy with the lowest Ru concentration (figure 1). With increase of Ru impurity, these positive diffuse islands expand at the expense of the negative ones. Given these features, the extraction of a diffuse moment is not straightforward. To a good approximation, we define the diffuse moment to be the moment resting on the faces of the Wigner-Seitz (WS) cell (one face of which is shown by the portion enclosed by broken straight lines in figures 1 to 3). Summing up the moment densities residing on all the faces of the WS cell faces we get the following diffuse moment per WS cell for the three alloys, in increasing order of Ru concentration: $+ (0\cdot016 \pm 0\cdot004)$ μ_B, $+ (0\cdot042 \pm 0\cdot004)$ μ_B and $+ (0\cdot039 \pm 0\cdot004)$ μ_B. In sharp contrast to what Mook observed in pure nickel, and to what other workers had observed in dilute *Ni-3d* alloys, the net diffuse moment in *Ni* Ru alloys is positive, tending to increase with Ru concentration.

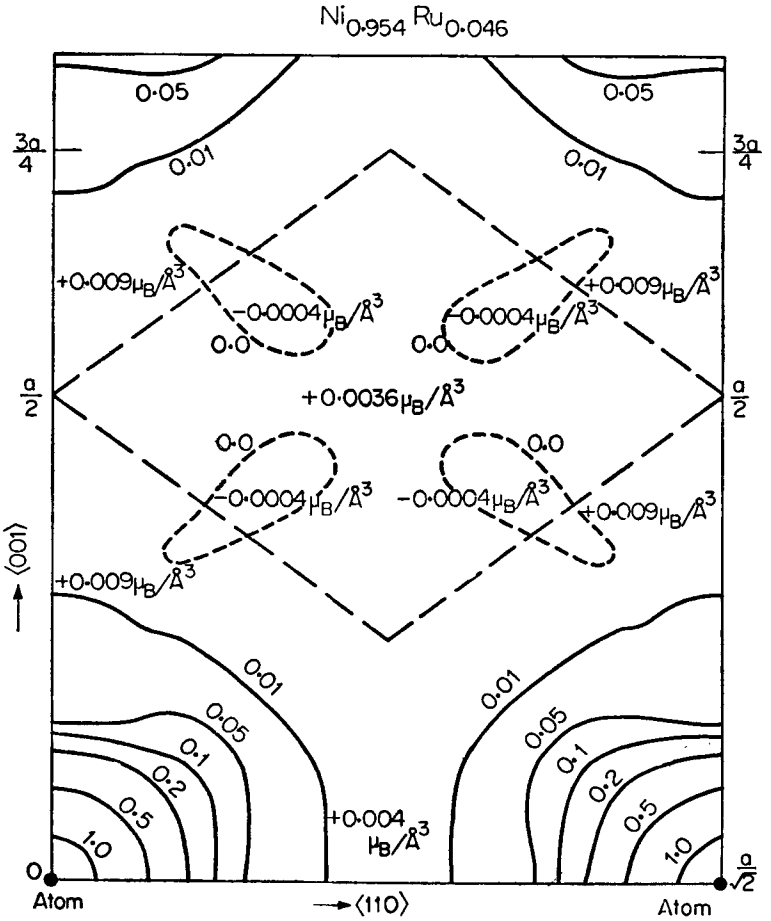

Figure 3. Magnetic moment density map in the $(1\bar{1}0)$ plane in $Ni_{0\cdot954}$ $Ru_{0\cdot046}$. The error on the diffuse density is $\pm$ 0·0004 $\mu_B/Å^3$.

3.2 *Spherically averaged local site moments*

A prescription to obtain the local site moment from the measured magnetic structure amplitudes themselves without recourse to bulk moment measurements was first given by Moon (1971). This essentially involves a Fourier sum of the magnetic structure amplitudes at a point $\mathbf{r}_B$ sufficiently far away from the atomic site. The local moment so obtained is however quite sensitive to the choice of $\mathbf{r}_B$ since it demands that the density around $\mathbf{r}_B$ should be zero or at least uniform. In I we had given an alternative method of evaluating the local site moment which is basically a modification of Moon's prescription. We recall equation (8) of our paper namely:

$$\mu'_{\text{loc}} = \frac{V_A}{V_0}\left[N\mu_{\text{loc}} + \sum_{j\neq 0}^{j_{\max}} M_j\, H\,(k_j R,\, 0)\right]. \tag{3}$$

V_0 is the unit cell volume containing N atoms, V_A is the volume of the averaging sphere of radius R, M_j is the magnetic structure amplitude measured at wave vector transfer k_j. The procedure outlined in I to extract the spherical local moment using equation (3) was carried out. Thus from figure 4 the following local site moments for the three alloy concentrations are obtained: 0·492 μ_B, 0·453 μ_B and 0·388 μ_B.

The diffuse moment then is simply the difference between the computed local site moment and the measured bulk moment. This is shown in column 4 of table 4. In the last column of this table are shown the diffuse moments got by summing up the magnetic contours on the WS cell faces alone. Both these columns clearly show the diffuse moments to be positive, with a tendency to increase with Ru concentration. It is pertinent to point out, however, that the difference in the value of these two sets of diffuse moments is due to the fact that one is representative of the diffuse moment over the entire unit cell volume while the other reflects the diffuse moment resting on the surface of the WS cell.

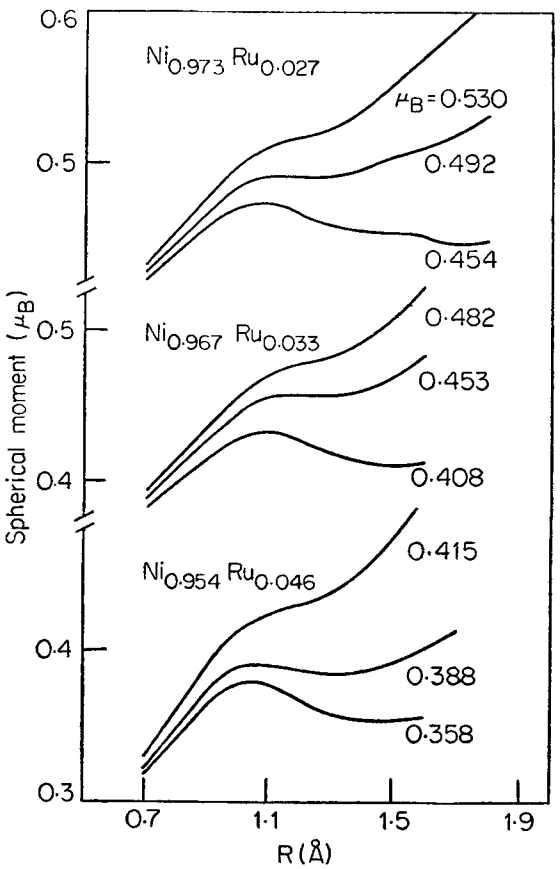

Figure 4. Spherically-averaged local moment plotted as a function of the radius R of the averaging sphere for all the three alloys and for various input values of μ_{loc} indicated on each curve.

Table 4. Summary of the comparison of the diffuse moments in the three alloys obtained from the density maps and from the evaluation of the local site moment and bulk moment measurement.

Impurity concentration	Bulk moment (μ_B)	Local moment (μ_B)	Diffuse moment (μ_B)	Diffuse moment from density maps (μ_B)
0·027	0·505	0·492	0·013	0·016
0·033	0·473	0·453	0·020	0·042
0·046	0·404	0·388	0·016	0·039

3.3 *Spherically averaged site form factors*

Spherically-averaged site form factors were computed directly from the measured magnetic structure amplitudes using equation (23) of Moon (1971), and these are shown in figure 5. These form factors have been normalised to the local site moments obtained in § 3.2. Also shown in this figure is the spherically-averaged form

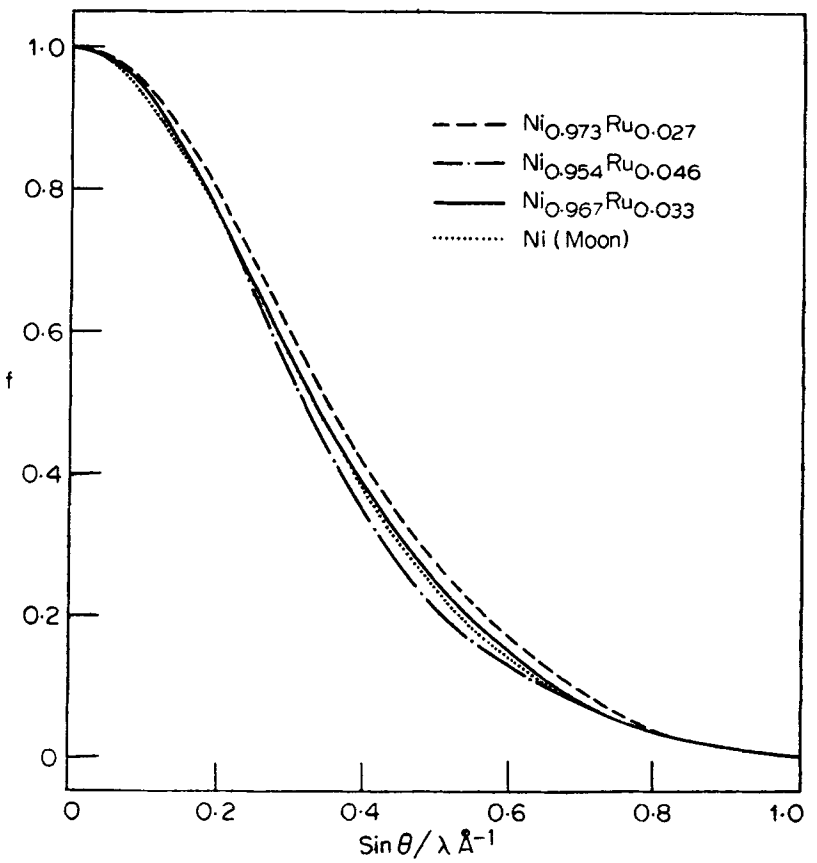

Figure 5. Spherical-averaged site form factors for the three alloy concentrations. The spherically-averaged form factor of pure Ni (Moon 1971) is shown as a dotted line. Note that all these form factors are normalised to their respective local moments.

factor for pure Ni (Moon 1971) which has been normalised to the Ni local moment of $0{\cdot}67\mu_B$. It is seen from this figure that compared to the Ni form factor, the site form factor for the alloy with the lowest Ru concentration is *broader*, then is almost the same for the next alloy and finally becomes *sharper* for the alloy with the largest Ru concentration. These features are vividly brought out in figure 6 where $\triangle f$, the difference between the spherical form factors of the alloy and nickel are plotted as function of $\sin\theta/\lambda$ for all the three concentrations. Since the form factors of the 4*d* elements are expected to be sharper than those of the 3*d* elements, the shape of the site form factor will be sensitive to the sign and magnitude of the 4*d* (Ru) moment. This is clear from the following expression in which the spherical site form factor is expressed in terms of the spherical form factors of the nickel host and the ruthenium impurity

$$f^{\mathrm{sp}}_{\mathrm{site}} = \frac{(1-c)}{\mu_{\mathrm{site}}}\mu_{\mathrm{Ni}}\, f^{\mathrm{sp}}_{\mathrm{Ni}} + \frac{c\,\mu_{\mathrm{Ru}}}{\mu_{\mathrm{site}}} f^{\mathrm{sp}}_{\mathrm{Ru}}. \tag{4}$$

It is seen from equation (4) that the shape of the site form factor will not reflect the sign of the impurity moment, if the host and impurity form factors are the same or very nearly the same as in the case of the 3*d*—3d dilute ferromagnetic alloys. In the *Ni* Ru system studied here, the broader spherical site form factor in the alloy of lowest Ru content does indeed point out to a negative moment on the Ru site and with increase of Ru content, this moment suffers a reversal of sign, when the spherical site form factor now becomes sharper than that in nickel. It needs to be emphasised that this rather startling evidence for a reversal of sign of the Ru moment over a small concentration range is not based on any model-dependent analysis but stems from a simple yet general consideration of the relative spatial extensions of the 3*d* and 4*d* orbitals. To pursue this feature, in the next section we analyse the measured magnetic structure amplitudes in terms of a linear combination of the effects coming from the host and impurity moments.

3.4 *Form factor analysis in terms of host and impurity moments*

We express the magnetic structure amplitude (in μ_B/atom)

$$M_{hkl} = (1-c)\mu^{\mathrm{loc}}_{\mathrm{Ni}}\left[\, f^{\mathrm{sp}}_{\mathrm{Ni}} + \frac{2}{g} A_{hkl}\left(\frac{5}{2}\alpha - 1\right)\langle j_4\rangle_{\mathrm{Ni}}\,\right] + c\mu^{\mathrm{loc}}_{\mathrm{Ru}}\, f^{\mathrm{sp}}_{\mathrm{Ru}}, \tag{5}$$

c is the Ru concentration, $f^{\mathrm{sp}}_{\mathrm{Ni}}$ and $f^{\mathrm{sp}}_{\mathrm{Ru}}$ are the spherical form factors for the respective atoms, $\mu^{\mathrm{loc}}_{\mathrm{Ni}}$ and $\mu^{\mathrm{loc}}_{\mathrm{Ru}}$ are the mean local moments for the host and impurity in the alloy. The second term in the square bracket in (5) reflects the asphericity of the host form factor due to the crystal environment. α is a measure of the moment density population in the E_g crystal field levels of the nickel host. We used the experimental spherically -averaged Ni form factor given by Moon (1971) for $f^{\mathrm{sp}}_{\mathrm{Ni}}$. In the absence

of any theoretical or experimental form factor for Ru, the experimentally determined spherical form factor of Pd was used (Cable *et al* 1975). $\langle j_4 \rangle_{Ni}$ were obtained from the H-F calculations of Watson and Freeman (1961) for Ni^{2+} and g the gyromagnetic ratio for *Ni* was taken to be 2·19.

For each of the alloy concentrations, the magnetic structure amplitudes were least squares fitted with equation (5), with three disposable parameters viz. μ_{Ni}^{loc}, μ_{Ru}^{loc} and α. Table 5 assembles the results of this analysis. One clearly sees evidence for the reversal of the sign of the impurity moment across the small concentration range and independently corroborates the conclusion got from the relative shapes of the site form factors in § 3.3. In this analysis, the site moment is defined to be equal to $(1-c)\mu_{Ni}^{loc} + c\mu_{Ru}^{loc}$ and is shown in the last column of table 5. The values of these site moments are in excellent agreement with those obtained from the prescription outlined in § 3.2.

3.5 *Form factor analysis in terms of site spin and orbital moments*

In this approach, we express the magnetic structure amplitude (in μ_B/atom) in terms of the site spin moment and the site orbital moment with their appropriate form factors:

$$M_{hkl} = \mu_{spin}^{site} f_{spin}^{site} + \mu_{orb}^{site} f_{orb}^{site} + \mu_{diff} f_{diff}. \tag{6}$$

Since $f_{diffuse}$ is expected to be a near ∂-function centred around (000), the last term in (6) makes no contribution to the measured magnetic structure amplitude. One can express the site orbital moment as

$$\mu_{orb}^{site} = \frac{g-2}{g} \mu_{bulk}$$

where μ_{bulk} is got from magnetization measurement. f_{spin}^{site} will contain a spherical and an aspherical part. To begin with, we do not know the site (spin and orbital) form factors in the Ni Ru systems and therefore to a good approximation, we use the nickel form factors themselves (Moon 1971). Equation (6) is then recast as

$$M_{hkl} = \mu_{spin}^{site} \left[f_{Ni}^{sp} + A_{hkl} \left(\frac{5}{2} \alpha - 1 \right) \langle j_4 \rangle_{Ni} \right] + \frac{g-2}{g} \mu_{bulk} f_{Ni}^{orb}. \tag{7}$$

Table 5. Summary of the analysis of the magnetic structure amplitude in terms of the host and impurity moments (§3.4).

Impurity concentration	Host moment (μ_B)	Impurity moment (μ_B)	Host moment asphericity α	Site moment (μ_B)
0·027	0·584(4)	−3·4(4)	0·16(1)	0·473(14)
0·033	0·484(3)	−0·26(16)	0·18(1)	0·459(8)
0·046	0·357(4)	+1·1(2)	0·22(2)	0·391(13)

$\langle j_4 \rangle_{Ni}$ are the HF form factors of Ni^{2+} (Watson and Freeman 1961). The observed magnetic structure amplitude were least squares fitted with (7) for all the three alloy concentrations, with two disposable parameters namely μ_{spin}^{site} and the asphericity parameter α. Tables 6 to 8 summarise the results of this analysis while in figures 7 to 9 are shown the observed and calculated magnetic structure amplitudes. The fits for all these three alloys are seen to be good. It is interesting to observe that the asphericity of the site moment increases initially and then softens out with increase of Ru concentration. As remarked earlier, this feature is also revealed in the moment density maps.

The site moment will be the sum of the spin site moment and the orbital site moment, with the former being about ten times as large as the latter. It will be instructive to compare the site moments obtained from this least squares analysis with the ones obtained directly, as described in § 3·2 for the three alloys. The present least squares analysis yields the following values for the site moment: 0 527 μ_B, 0·463 μ_B and 0·356 μ_B while those obtained by direct evaluation (§ 3.2) are: 0·492 μ_B, 0 453 μ_B and 0 388 μ_B. Clearly, the least squares fit from (7) gives a *larger* site moment for the alloy of lowest Ru concentration, and a *smaller* site moment for the alloy of highest Ru concentration and about the same site moment for the alloy of inter-

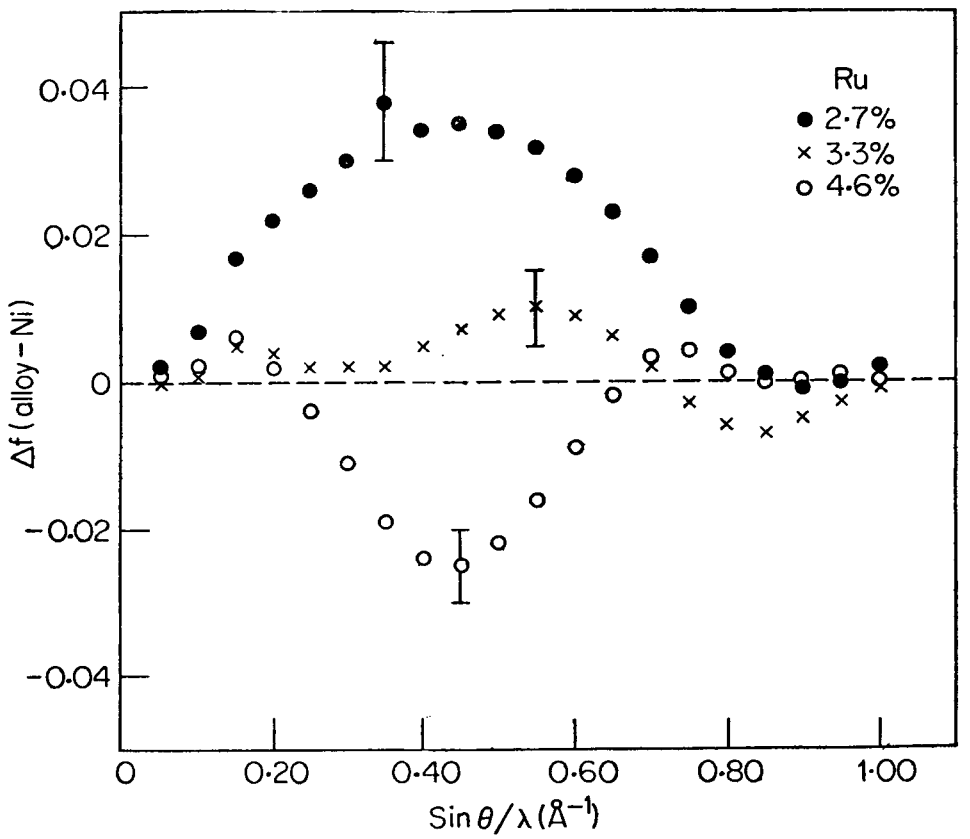

Figure 6. The difference Δf of the alloy form factor and Ni form factor plotted as a function of sin θ/λ.

Table 6. Summary of the magnetic structure amplitude (in μ_B/atom) for $Ni_{0.973}Ru_{0.027}$ at room temperature.

hkl	sin θ/λ	M_{obs}	M^*_{cal}
111	0·2462	0·347(3)	0·357
200	0·2843	0·301(3)	0·308
220	0·4021	0·199(2)	0·202
311	0·4715	0·150(2)	0·142
222	0·4925	0·160(2)	0·144
400	0·5687	0·076(3)	0·066
331	0·6197	0·084(3)	0·077
420	0·6358	0·050(3)	0·058
422	0·6965	0·058(3)	0·050
511	0·7387	0·022(2)	0·016
333	0·7387	0·052(2)	0·051
440	0·8042	0·022(4)	0·027
531	0·8411	0·016(4)	0·016
600	0·8530	(−)0·019(6)	(—)0·014
442	0·8530	0·030(3)	0·026
620	0·8991	(—)0·001(5)	(—)0·0007

$$M^*_{cal} = \mu^{site}_{spin}\left[f^{sp}_{Ni} + A_{hkl}\left(\frac{5}{2}\alpha - 1\right)\langle j_4\rangle_{Ni}\right] + \frac{g-2}{g}\mu_{Bulk}f^{orb}_{Ni}$$

$$\mu^{site}_{spin} = (0{\cdot}485 \pm 0{\cdot}001)\mu_B;\ \alpha = 0.156 \pm 0{\cdot}006$$

Table 7. Summary of the magnetic structure amplitude (in μ_B/atom) for $Ni_{0.967}Ru_{0.033}$ at room temperature.

hkl	sin θ/λ	M_{obs}	M^*_{cal}
111	0·2450	0·304(3)	0·314
200	0·2829	0·278(2)	0·272
220	0·4001	0·170(3)	0·178
311	0·4691	0·130(2)	0·126
222	0·4900	0·131(2)	0·126
400	0·5658	0·061(2)	0·063
331	0·6165	0·067(2)	0·069
420	0·6326	0·051(2)	0·052
422	0·6929	0·046(2)	0·044
511	0·7350	0·017(1)	0·017
333	0·7350	0·043(2)	0·044
440	0·8001	0·0241(3)	0·024
531	0·8638	0·011(3)	0·015
600	0·8487	(—)0·014(3)	(—)0·009
442	0·8487	0·017(2)	0·022
620	0·8946	(—)0·003(3)	(—)0·004

$$M^*_{cal} = \mu^{site}_{spin}\left[f^{sp}_{Ni} + A_{hkl}\left(\frac{5}{2}\alpha - 1\right)\langle j_4\rangle_{Ni}\right] + \frac{g-2}{g}\mu_{Bulk}f^{orb}_{Ni}$$

$$\mu^{site}_{spin} = (0{\cdot}422 \pm 0{\cdot}001)\mu_B;\ \alpha = 0{\cdot}184 \pm 0{\cdot}007$$

Table 8. Summary of the magnetic structure amplitudes (in μ_B/atom) for $Ni_{0.954}$ $Ru_{0.046}$ alloy at room temperature.

hkl	sin θ/λ	M_{obs}	M^*_{cal}
111	0·2450	0·2501(1)	0·242
200	0·2829	0·224(2)	0·211
220	0·4001	0·141(2)	0·137
311	0·4691	0·092(1)	0·098
222	0·4900	0·089(1)	0·096
400	0·5658	0·053(2)	0·053
331	0·6165	0·050(1)	0·051
420	0·6326	0·043(2)	0·042
422	0·6929	0·034(1)	0·034
511	0·7350	0·015(1)	0·016
333	0·7350	0·033(1)	0·031
440	0·8001	0·021(1)	0·018
531	0·8368	0·015(4)	0·012
600	0·8487	(−)0·007(3)	(−)0·002
442	0·8487	0·017(1)	0·015
620	0·8946	(−)0·003(3)	(−)0·001

$$M^*_{cal} = \mu^{site}_{spin}\left[f^{sp}_{Ni} + A_{hkl}\left(\frac{5}{2}\alpha - 1\right)\langle j_4\rangle_{Ni}\right] + \frac{g-2}{g}\,\mu_{bulk}\,f^{orb}_{Ni}.$$

$\mu^{site}_{spin} = (0{\cdot}322 \pm 0{\cdot}002)\ \mu_B$; $\alpha = 0{\cdot}24 \pm 0{\cdot}02$

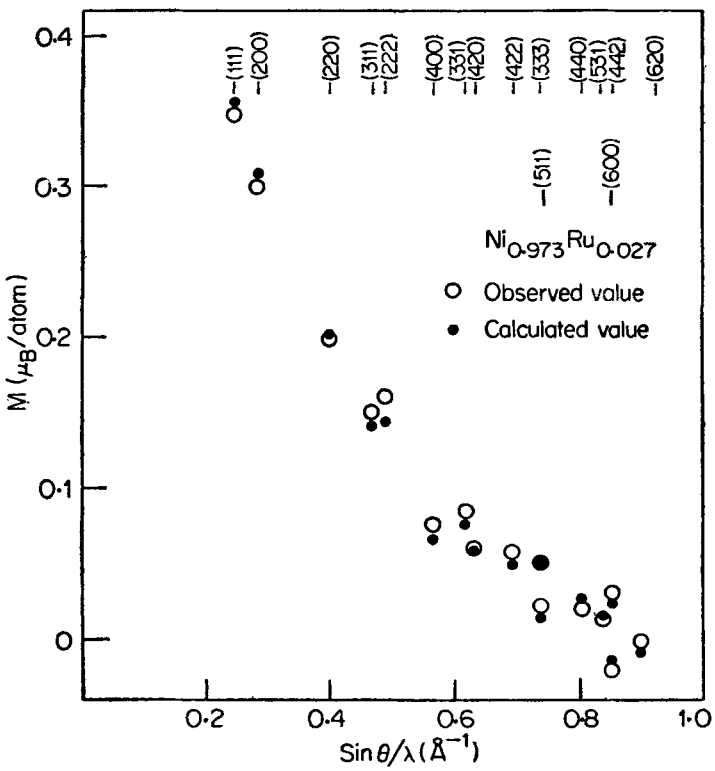

Figure 7. Comparison of the observed (open circles) and calculated (solid circles) magnetic structure amplitudes (μ_B/atom) for $Ni_{0.973}$ $Ru_{0.027}$ (equation (7)).

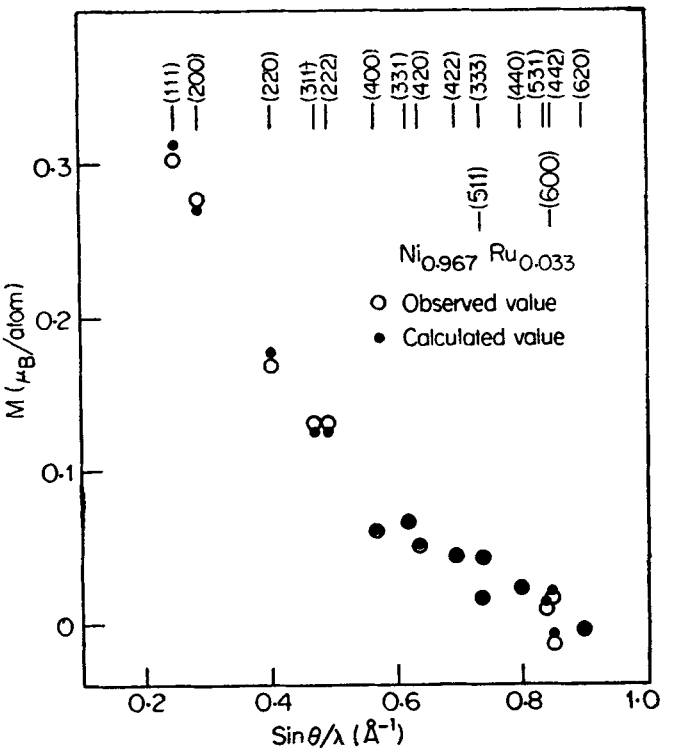

Figure 8. Comparison of the observed (open circles) and calculated (solid circles) magnetic structure amplitudes (μ_B/atom) for $Ni_{0.967}$ $Ru_{0.033}$ (equation (7)).

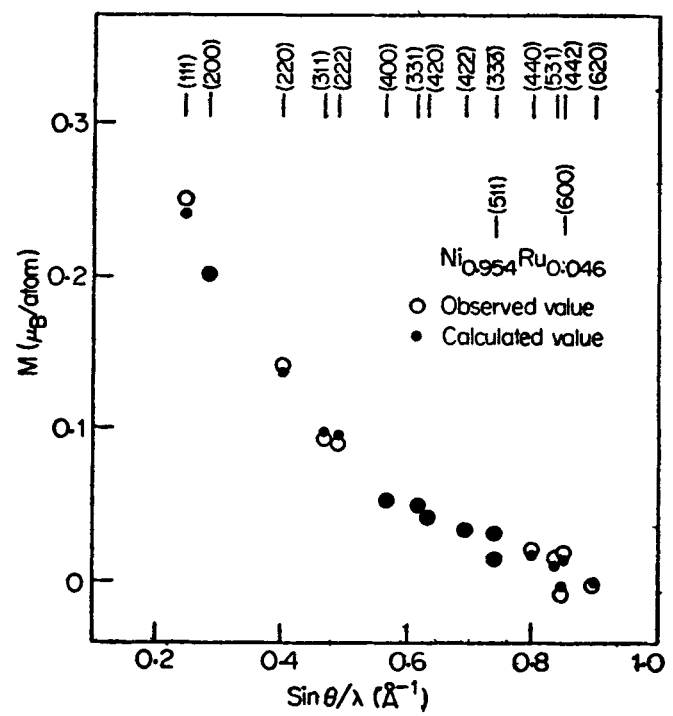

Figure 9. Comparison of the observed (open circles) and calculated (solid circles) magnetic structure amplitudes (μ_B/atom) for $Ni_{0.954}$ $Ru_{0.046}$ (equation (7)).

mediate composition than the corresponding true site moment. This apparent discrepancy is not accidental but physically significant in as much as it is related closely to the shapes of the Ni spin form factors used in the least squares fit (equation (7)) in place of the true site form factors. In fitting the data using (7), a broader spin form factor would reduce the μ_{spin}^{site} value (for the alloy with the lowest Ru concentration) and similarly, a sharper spin form factor would enhance the μ_{spin}^{site} value for the alloy with the largest Ru concentration, and thus wipe out the apparent discrepancy observed. Thus, complete compatibility between the two sets of site moment values can be established only if we demand that the site form factor for the alloy with 2·7 at % Ru is broader than that in Ni, eventually becomes sharper than that in Ni for the alloy with 4·6 at % Ru. This analysis confirms again the independent evidence established earlier in § 3.3 regarding the shape of the site form factors.

4. Discussion and Conclusion

The polarised neutron diffraction study carried on these three alloys of *Ni* Ru show that the introduction of the Ru impurity in the nickel matrix brings about extensive perturbations in the diffuse moment density (as revealed by the moment density maps)—the net diffuse moment being positive with a tendency to increase with increase of Ru impurity. Transport property measurements made on nickel-based alloys with dilute impurities of the 4*d* elements had shown a peaking of residual resistivity (Durand and Gautier 1970) and a reversal of the sign of the thermoelectric power (Cadeville and Roussel 1971) with Ru impurity. These authors had argued that these observations were compatible with the existence of an impurity virtual bound state (vbs) near E_f. Very recently, a multiband CPA calculation carried out by Chakravarthy and Madhav Rao (1980) show, amongst other things, that the Ru density of states are highly localised around E_f simulating a vbs. Since a vbs situated at E_f is expected to introduce spatially well-extended moment perturbations, the strong modification in the diffuse moment density revealed in the present study is consistent with this picture. Widespread perturbations around the Ru site have been seen earlier from unpolarised and polarised neutron diffuse scattering (Comly *et al* 1968; Parette and Kajzar 1979).

However, as argued by us in § 3, the shapes of the spherically-averaged site form factors and the magnetic form factor analyses seem to suggest a reversal of the sign of the Ru moment, from negative to positive, over a small concentration range. The multiband CPA calculations, referred to earlier, predict the Ru moment to be negative at very dilute concentration, decreasing very sharply with increasing Ru concentration, without suffering however, a sign reversal. Diffuse neutron scattering studies have shown no evidence of chemical or magnetic clustering in *Ni* Ru around the concentration range. While it can be said that very strong local environmental effects are probably responsible for such a sign reversal, this experimental feature cannot be explained in the framework of existing models. On the other hand, the possibility of *Ni* Ru existing as a pseudoternary *magnetic* system cannot be completely ruled out, with the Ru atom having two types of magnetic moments, one parallel to and the other antiparallel to the host magnetization. *Ni* Mn has been experimentally shown to be such a pseudoternary system (Kitaoka and Asayama 1976). Because

of the rather severe influence the Ru atom has over the first three or four neighbour shells of the Ni host, we can expect the interactions between Ru-Ru neighbour pairs to have a greater range since these effects occur through the strongly perturbed nickel matrix rather than as a direct impurity-impurity interaction. As a consequence of these rather complex interactions, it is probable that the relative proportions of the parallel and antiparallel Ru moments change over a small concentration range, thus simulating as apparent spin reversal as seen from our present study. A detailed spin-echo NMR investigation (with and without an external magnetic field) in the *Ni* Ru system may clarify this intriguing feature.

5. Acknowledgements

We are grateful to Dr P K Iyengar for his encouragement and interest in this study. We thank Prof. D C Khan of IIT. Kanpur for carrying out the bulk moment measurements on the samples. One of us (LMR) warmly thanks Dr G Parette of CEN de Saclay, France for the loan of the crystals and for fruitful correspondence. Dr Z Jirak participated in the initial stage of this experimental study and we thank him. The technical help of Mr B S Srinivasan is gratefully acknowledged.

References

Cable J W, Wollan E O, Felcher G P, Brun T O and Hornfeldt S P 1975 *Phys. Rev. Lett.* **34** 278
Cadeville M C and Roussel J 1971 *J. Phys.* **F1** 686
Chakravarthy R and Madhav Rao L 1980 (to be published)
Comly J B, Holden T M and Low G G 1968 *J. Phys.* **C1** 458
Dobrzynski L, Maniswski F, Modrzewski A and Sikorsk D 1970 *Phys. Status Solidi* **28** 103
Durand J and Gautier F 1970 *J. Phys. Chem. Solids* **31** 2773
Ito Y and Akimitsu J 1974 *J. Phys. Soc. Jpn.* **36** 431
Kitaoka Y and Asayama K 1976 *J. Phys. Soc. Jpn.* **40** 1521
Livet F and Radhakrishna P 1976 *Solid State Commun.* **18** 331
Madhav Rao L, Chakravarthy R, Jirak Z and Satya Murthy N S 1978 *Phys. Rev.* **B18** 6275
Mook H A 1966 *Phys. Rev.* **148** 495
Moon R M 1964 *Phys. Rev.* **136** A195
Moon R M 1971 *Int. J. Magn.* **1** 219
Parette G and Kajzar F 1979 *J. Phys.* **F9** 1807
Shull C G and Yamada Y 1962 *J. Phys. Soc. Jpn. Suppl.* **17** 1.
Watson R E and Freeman A J 1961 *Acta Crystallogr.* **14** 27.